Research Report

98-31

Transient Modeling and Analysis of Motor Terminal Voltage on PWM Inverter-Fed AC Motor Drives

E. Zhong*, T.A. Lipo, S. Rossiter*

Wisconsin Power Electronic
Research Center
University of Wisconsin-Madison
Madison WI 53706-1691

*Energy Management Corporation
60 W. Burton Avenue
Salt Lake City, UT 84115

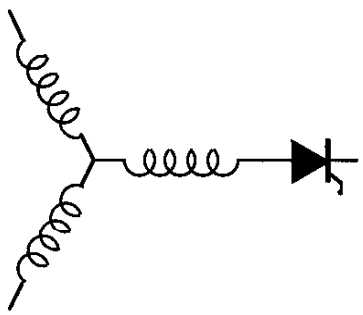

Wisconsin
Electric
Machines &
Power
Electronics
Consortium

University of Wisconsin-Madison
College of Engineering
Wisconsin Power Electronics Research Center
2559D Engineering Hall
1415 Engineering Drive
Madison WI 53706-1691

Transient Modeling and Analysis of Motor Terminal Voltage on PWM Inverter-Fed AC Motor Drives

Erkuan Zhong
Member IEEE
Energy Management
Corporation
60 W Burton Avenue
Salt Lake City, UT 84115 USA
email:
ezhong@sprintmail.com

Thomas A. Lipo
Fellow IEEE
Dept. of Electrical and
Computer Engineering
University of Wisconsin-
Madison
1415 Engineering Drive
Madison, WI 53706 USA
email: lipo@engr.wisc.edu

Steven Rossiter
Energy Management
Corporation
60 W Burton Avenue
Salt Lake City, UT 84115 USA
email:rossiter@earthlink.net

Abstract-This paper presents new concepts in the modeling and analysis of transient over-voltage and ringing associated with PWM inverter-fed AC machines. Experimental results are presented which demonstrate that frequency response (based on a typical AC induction machine's impedance) behaves like a capacitance-resistance network rather an inductance-resistance network in the high frequency range. Traveling wave reflection phenomena (as a result of the drive system) are analyzed considering motor capacitance. The following two transient stages are proposed to describe the motor voltage waveforms observed: 1) traveling wave reflection and 2) inductance-capacitance ringing. Criteria determining the maximum over-voltage at the motor terminals are discussed including design considerations for an artificial RC terminator. The analytical estimations and simulations for transient voltage based on the hypothesis are confirmed with both laboratory and field results.

1. INTRODUCTION

High speed switching devices including BJTs, MOSFETs, and IGBTs have been widely used in adjustable speed drives (ASDs). These devices have relatively low switching losses, allowing increased switching frequency resulting in improved ASD performance. However, with switching times now down to the 1μS range, new problems have become apparent. In long cable installations, over-voltage has been observed at the motor terminals thereby increasing stress on motor winding insulation and accelerating the insulation aging process [1]-[3]. Many efforts have been made to understand this problem and a number of techniques for over-voltage mitigation have been developed [4]-[7]. To date, most studies have been based on the popular "traveling wave reflection phenomena". This is explained as a (inverter initiated) voltage pulse being reflected at the motor terminal due to mismatching of surge impedance between the cable and the motor. Assuming the motor's surge impedance to be much higher than that of the cable, the reflected voltage is equal in magnitude and in-phase with the incident pulse. The resultant voltage can increase quickly up to two times the amplitude of the incident voltage. Furthermore, the motor's surge impedance was treated as resistive to determine the magnitude of wave reflection (e.g. the calculation of classical reflection coefficient).

The popular RC terminator network for suppression of over-voltage has been developed based on such impedance matching criteria. To this point, however, studies have failed to consider the high frequency range associated with the high *dv/dt* voltage when modeling a motor's characteristics. Also, other studies have not explained the effects of a terminated motor size on observed voltage ringing frequency, nor considered the moment when maximum over-voltage occurs. Lumped parameter models of cable-motor systems (considering stray capacitance of the motor) have been used in calculations for inverter output filters in the low frequency ranges. Lumped parameter models, however, can not apply to the analysis of circuits carrying surge current.

This paper presents new concepts in the modeling and analysis of over-voltage transients and the ringing associated with PWM inverter fed AC motors. The paper first discusses the PWM voltage spectrum with an emphasis on higher frequency components associated with each pulse edge. An experimental spectrum reveals significant power extending into the radio frequency (RF) range. By applying a frequency response concept to motor input impedance, it becomes clear that stray capacitance of the motor winding affects the frequency response so as to contain L-C-R network characteristics. In frequency ranges over one hundred kHz (RF range) the motor input impedance approaches that of a full capacitive network with resistive loss. From this result, it is obvious that the motor surge impedance assumption used in most studies [4]-[7] can no longer be true. Therefore, this paper's modeling of system components is based on the inverter voltage spectrum and the experimental frequency response of typical devices.

To illustrate the transient voltage of PWM drives two consecutive transient stages are proposed, i.e. traveling wave reflection and ringing. In the beginning stage, the cable is modeled as a transmission line terminated with the capacitance-resistance network of the proposed motor model. By applying transmission line equations with given boundary conditions the system transient voltages are

obtained analytically. In the following transient stage of ringing, however, the cable is modeled as a lumped parameter pi or T type circuit, while the motor remains capacitance-resistance. The transient voltages are thus illustrated as the basis of the proposed hypothesis along with experimental results. A new explanation of the popular RC cable terminator and its design consideration is discussed.

2. Modeling of Inverter-Cable-Motor System

A. PWM *inverter voltage spectrum*

The voltage waveform $v(t)$ from a typical PWM voltage source inverter may simply be described as a series of trapezoids with varying width. Characterization of $v(t)$ may also be given by means of its spectrum. The spectrum of a series of trapezoidal waveforms with constant width, as shown in Fig.1 (a), is

$$B_n = 2AD\frac{\sin n\pi D}{n\pi D}\frac{\sin n\pi \frac{t_r}{T}}{n\pi \frac{t_r}{T}}$$

where T is the pulse repetition period, $D=T_1/T$ the duty cycle with t_r the rise/fall-time. The spectral envelope of B_n gives a flat top line to the break point at frequency $1/\pi T_1$, then falls off at -20dB/decade until the frequency n/T reaches the value of $(1/\pi t_r)$. At this point the function of sinx/x related to rise-time t_r begins to contribute increasingly to the rate of roll-off to -40dB/decade. For a certain PWM pattern D, the shorter the rise-time t_r of the voltage pulse, the wider the bandwidth extends. Fig.1 (b) shows the experimental spectrum of a voltage waveform from a typical PWM transistor inverter. (230 V, 60 Hz, switching frequency 4 kHz, rise/fall time 0.15 μS). The spectrum reveals notable power extending into radio frequency (RF) range, e.g. 20 dBV(10V) at about 100 kHz falling to 3 dBV (1.4V) at 1 MHz, and a fraction of a volt over a few MHz, which generates high frequency currents in the motor as illustrated in later sections.

B. Modeling of cables

Although various physical distributed capacitance, resistance, and inductance exist, cable modeling may be approached with different circuits (depending on length of the cable, frequency of the current carried, amplitude of the voltage applied, and the terminated load). For transient analysis in ASD systems, both the "distributed parameter" model and the "lumped LCR" model should be employed.

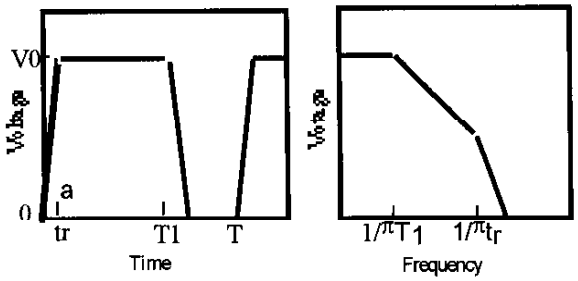

(a)

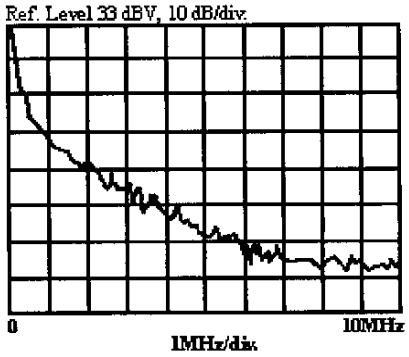

(b)

Fig. 1 Typical PWM VSI inverter output voltage. (a) Simplified pulse waveform and theoretical spectra. (b) Experimental voltage spectrum, from a typical PWM transistor inverter, 230 V, 60 Hz, switching frequency 4 kHz, rise/fall time 0.15 μS.

At the beginning stage, a pulse voltage is imposed on one end of the cable and propagates away resulting in the considerable variance of capacitive shunt currents along the cable. During the following stage, however, capacitive shunt current distribution is approximately even due to a considerable decrease of dv/dt (eventually to zero at the pulse top) so that a lumped circuit model may be applied to modeling of the cable. An experimental frequency response of cable parameters manifests a frequency distribution for which a lumped model can be applied as shown in Fig. 2. In the experiment a programmable LCR meter was used to measure the inductance and capacitance between cable conductors 45 meter in length, (3x AWG #14, 600 V THW). It is clear that lumped parameters may apply to the cable provided that the signal frequencies are much lower than the characteristic frequency of the cable with the corresponding quarter wave length equal to cable length (about 800 kHz for this test cable).

C. Modeling of AC induction motors

Traditional modeling of AC machines (resistance-inductance network) used to analyze cable-motor transient voltage results in the characterization of the motor

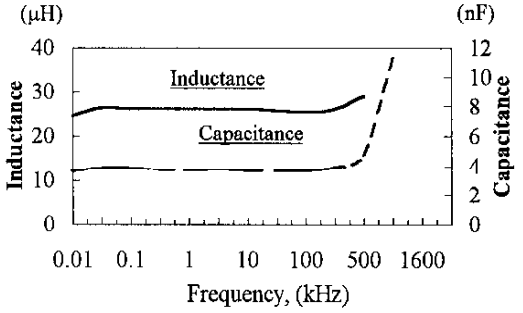

Fig. 2 Frequency dependency of parameters of 45 meter cable. 600 V, 3-wire #14 A.W.G.

windings as a very high impedance compared to the cable surge impedance. In addition, the motor input impedance is characterized to be resistive in order to calculate the reflection coefficient. However, a considerable portion of experimental waveform do not coincide with this model. For example, the maximum voltage peak does not appear as a function of only the incident wave but rather varies with the motor size and type. The ringing frequency of the voltage, for example, not only depends on the cable length but also on the motor size. Therefore, proper modeling of the AC machine has a significant effect in respect to an understanding of transient over-voltage in AC drive systems.

The effects of stray capacitance on motor behavior has been recognized in recent years as the cause of the leakage ground current [9][10], on harmonics loss[11], on motor bearing current [12] and on Electromagnetic Interference [13][14]. All of these issues are concerned with the behavior of the motor responding to frequencies above several kilohertzs. Since the bandwidth of the voltage being applied to the motor extends into the radio frequency (RF) range as previously mentioned, the frequency characteristic of the motor input impedance at a wider frequency range must be explored. In order to consider the effects of stray capacitance, a simplified modeling of motor stator windings for radio frequencies has been proposed by the authors as shown in Fig. 3 [13]. In this model a typical 3-phase motor is characterized as an L-C-R network. An estimation of model parameters must also be performed by comparing experimental results with the model's computer simulation results in the frequency domain, (e.g. frequency dependency of input impedance for the same motor. The experimental results are presented in Fig. 4 (a) and (b) on two three-phase induction motors rated 2.2 kW and 7.5 kW, respectively. Test connections were made to simulate the operation of an inverter fed motor. The impedance Z, phase angle θ, inductance L, and capacitance C are measured by a programmable LCR meter. The

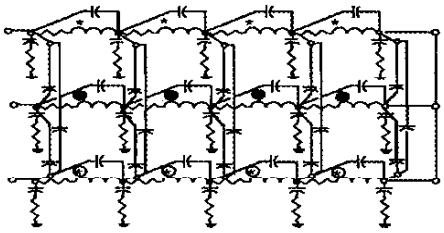

Fig. 3 Model of 3-phase induction motor for radio frequency including parasitic capacitance, [13].

experimental results can be summarized as follows: First, there exists a primary resonant frequency at 160 kHz for the 2.2 kW and at 60 kHz for the 7.5 kW motor, respectively. With increasing frequency, the impedance is inductive over the low frequency range and it increases in magnitude to a few kilohms until resonance. Above the resonant frequency, however, the impedance is essentially capacitive decreasing in magnitude to a few tens of ohms. 2) In addition to the primary resonance there is a second resonance with a smaller peak magnitude at higher frequencies. 3) At frequencies sufficiently higher than the second resonant frequency the capacitive component of the impedance varies so little that it may be approximately treated as a single capacitance, (e.g. 0.2 nF for the 2.2 kW

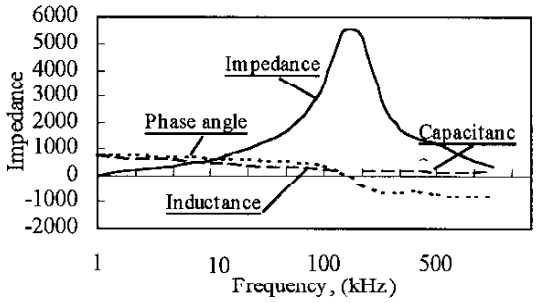

(a)

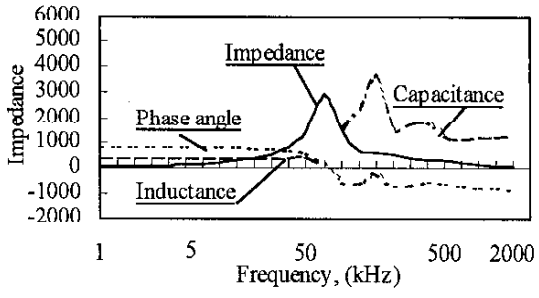

(b)

Fig. 4 Experimental frequency dependency of input impedance of typical 3-phase induction motors, impedance, 1Ω/div.; phase angle, 0.1°/div.; inductance, 10 μH/div.; capacitance, 1pF/div. (a) 2.2 kW motor. (b) 7.5 kW motor

motor and 1.2 nF for the 7.5 kW motor). The value of this equivalent capacitance is a fraction (about 1/3) of the total capacitance of the three windings of the motor with respect to its frame. 4) Resistive loss exists in the entire frequency range. The experimental errors caused by test conditions, however, should occur in the low frequency range as well as shifting the point of resonance. The simulation frequency dependency based on the model shown in Fig. 3 (including distributed capacitance) approaches the experimental result [13].

The proposed modeling of drive systems has been used by the authors for system simulations to predict the transient voltage waveform where the cable is modeled as transmission line while the motor is modeled as an L-C-R network. As shown in Fig. 5, simulation voltage waveforms closely approximate to the experimental voltage waveforms of the two induction motors. The effects of motor size on the transient voltage waveform can be verified.

3. Analytical Transient Voltage of Motor Terminals

In order to understand how the motor stray capacitance affects the transient voltage (peak value and ringing frequency), analytical methods can provide insight into understanding the transient phenomena. Further simplification of the motor model is necessary for such an analysis. Based on the experimental results, the drive system can be simplified as shown in Fig. 6.

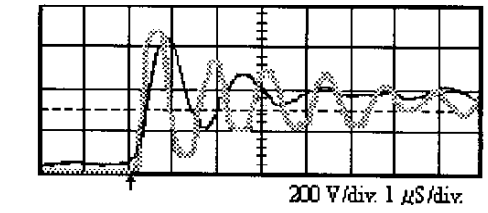

(a)

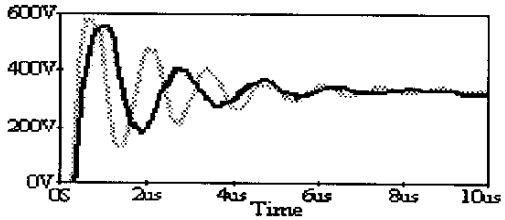

(b)

Fig. 5 Voltage waveform of motor terminal, (a) experimental, (b) Simulation based on 2.2 kW motor (light line) and on 22 kW motor (dark line), both machines are fed by PWM inverter via 45 meter cable.

That is: a) the analysis is performed for the response of the motor to only a single pulse voltage, b) a capacitance-resistance circuit (R, C) is used to model the motor windings because the frequency band of the imposed voltage with high *dv/dt* is far beyond that of the motor resonant frequency, c) the motor cable is treated as a loss-less transmission line, d) the inverter output pulse waveform is piecewise linear, as shown in Fig. 1 (a), without distortion when first arriving at the motor terminal.

The lossless transmission line equations are:

$$\frac{\partial v}{\partial x} = -L_0 \frac{\partial i}{\partial t} \quad (1a), \qquad \frac{\partial i}{\partial x} = -C_0 \frac{\partial v}{\partial t} \quad (1b),$$

where x is the distance between the point x and the cable end, $v(x,t)$ is the voltage at x, $i(x,t)$ is the current at x, L_0 is the inductance per unit length and C_0 is the capacitance per unit length, respectively. The solution of (1a) and (1b) for v (or i) implies that v (or i) is the sum of the forward traveling wave $v_{(+)}$ (or $i_{(+)}$) and the backward traveling wave $v_{(-)}$ (or $i_{(-)}$). Both propagate along the line at a speed u, with voltage and current related in terms of surge impedance Zo, as given in the following equations:

$$u = \frac{1}{\sqrt{L_0 C_0}} \quad (2), \qquad Z_0 = \sqrt{\frac{L_0}{C_0}} \quad (3),$$

$$v_{(+)} = Z_0 i_{(+)} \quad (4), \qquad v_{(-)} = Z_0 i_{(-)} \quad (5),$$

Therefore, as the first single incident wave ($v_{(+)}$, $i_{(+)}$) (assumed to be the inverter pulse output) arrives at the motor terminals, load current (i_c) flows into load (R, C) and a reflection wave ($v_{(-)}$, $i_{(-)}$) is produced due to impedance mismatch between the transmission line and the termination load (R, C). Applying Kirchoff's laws to the terminal (node A) as shown in Fig. 6, the following applies:

$$v = v_{(+)} + v_{(-)} \quad (6), \qquad i_{(+)} = i_c + i_{(-)} \quad (7)$$

and

$$v_c = i_c R + \frac{1}{C}\int i_c dt \quad (8)$$

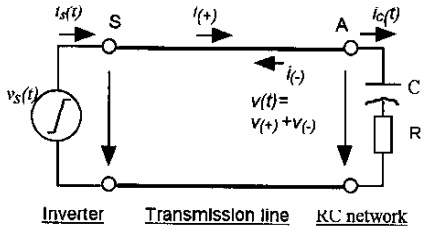

Fig. 6 Simplified inverter-cable-motor system model 1.

As Z_o, R and C are known, and given $v_{(+)}=v_s(t)$, (assumed as the inverter output voltage shown in Fig.1 (a), the following simultaneous differential equations, (4), (5), (6), (7). (8) can be solved with the initial conditions. Therefore the first reflected wave ($v_{(-)}$, $i_{(-)}$) as well as the node A voltage $v(t)$ during this period can be obtained. The solution is summarized as follows:

The Laplace transforms of (4) to (8) under zero initial conditions, i.e., $v_c(0)=0$ will be as defined in (9) to (13), respectively.

$$V_{(+)}(s) = Z_0 I_{(+)}(s) \tag{9}$$

$$V_{(-)}(s) = Z_0 I_{(-)}(s) \tag{10}$$

$$V(s) = V_{(+)}(s) + V_{(-)}(s) \tag{11}$$

$$I_{(+)}(s) = I_c(s) + I_{(-)}(s) \tag{12}$$

$$V(s) = RI_c(s) + \frac{1}{sC} I_c(s) \tag{13}$$

where variable s is generally a complex valued. From (9) to (13), solving for $V_{(-)}(s)$ we have:

$$V_{(-)}(s) = \frac{1+C(R-Z_0)s}{1+C(R+Z_0)s} V_{(+)}(s) \tag{14}$$

As $v_{(+)}=v_s(t)$, is known as in Fig.1 (a) and can be expressed as:

$$v_{(+)}(t) = \frac{V_0}{a} tu(t) - \frac{V_0}{a}(t-a)u(t-a) \tag{15}$$

where $u(t)$ and $u(t-a)$ are step functions, i.e., while $t<0$, both $u(t)$ and $u(t-a)$ are zero; while $0<t<a$, $u(t)=1$ and $u(t-a)=0$, while $a<t$, both $u(t)=1$ and $u(t-a)=1$. Since the Laplace transform of $v_{(+)}(t)$, (15), is

$$V_{(+)}(s) = \frac{V_0(1-e^{-sa})}{s^2 a} \tag{16}$$

Substituting (16) into (14), the Laplace transform of the reflection voltage $v_{(-)}(t)$ becomes

$$V_{(-)}(s) = \frac{V_0}{a}\left[\frac{1}{s^2} - \frac{2CZ_0}{s} + \frac{2C^2 Z_0(R+Z_0)}{1+sC(R+Z_0)}\right] - \frac{V_0}{a} e^{-sa}\left[\frac{1}{s^2} - \frac{2CZ_0}{s} + \frac{2C^2 Z_0(R+Z_0)}{1+sC(R+Z_0)}\right] \tag{17}$$

The reflection voltage wave $v_{(-)}(t)$ is then obtained with reverse Laplace transform of $V_{(-)}(s)$, (17),

$$v_{(-)}(t) = \frac{V_0}{a}\left[t - 2CZ_0\left(1-e^{-\frac{t}{C(R+Z_0)}}\right)\right]u(t) - \frac{V_0}{a}\left[(t-a) - 2CZ_0\left(1-e^{-\frac{t-a}{C(R+Z_0)}}\right)\right]u(t-a) \tag{18}$$

where $u(t)$ and $u(t-a)$ are step functions as mentioned above. Therefore, the motor terminal total voltage $v(t)$, the sum of the incident wave and the reflected wave can be obtained analytically, i.e., $v(t)= v_{(+)}(t)+ v_{(-)}(t)$

$$v(t) = \frac{V_0}{a}\left[2t - 2CZ_0\left(1-e^{-\frac{t}{C(R+Z_0)}}\right)\right]u(t) - \frac{V_0}{a}\left[2(t-a) - 2CZ_0\left(1-e^{-\frac{t-a}{C(R+Z_0)}}\right)\right]u(t-a) \tag{19}$$

From (18) and (19) the following can be noted: 1) The reflected wave $v_{(-)}(t)$ in (18) increases exponentially and is less than the incident wave, i.e. $0<v_{(-)}(t)<v_{(+)}(t)$. This fact is due to the charging of terminated capacitance C. The terminal voltage $v(t)$ is still higher than the incident voltage $v_{(+)}(t)$, as well as the dv/dt. 2) While $a<t$, however, terminal voltage $v(t)$ ramps up much slower in reaching of $2V_0$ at about $t=(3\sim4)C(R+Z_0)$, provided there is not a consecutive incident voltage wave arriving. 3) With R equal to infinity (open circuit termination) the voltage $v(t)$ will reach the maximum $2V_o$ at $t=a$, synchronous with the incident wave. Consequently, the capacitive reactance terminated with the transmission line yields distinctly different responses than with resistance termination. Shown in Fig. 7, are the analytical traces of the voltages for a given circuit, where voltage amplitude V_o=320 V, rise time a=0.15 μS, surge impedance of transmission line Z_o=100 Ω, capacitance C=0.002 μF and R=150 Ω.

From the above discussion, the analytical expression for terminal voltage $v(t)$ is derived for a very short period, in that the length of the transmission line is long enough so that no consecutive incident wave arrives resulting in exponentially increasing of the voltage up to twice the amplitude of the incident voltage. For a limited length of cable, the first reflection wave will travel backward to the other end and cause a new reflected wave at that terminal to again return forward to the motor terminal. This would be referred to as the second incident wave, which is superimposed on the voltage already existing at the terminal.

Termination of the cable on the inverter side is completely different from that on the motor side as there is a large, smooth capacitance due to the dc link so that $v_s=V_0$=constant. Applying Kirchoff's law and

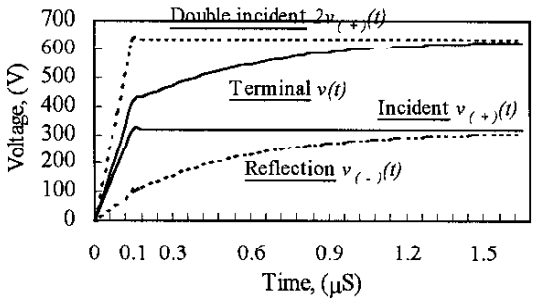

Fig. 7 Analytical terminal waveforms, incident pulse 320 V, rise-time 0.15 μS, cable $Z_0=100\ \Omega$, termination $R=150\ \Omega$, C=2 nF.

transmission line theory on the terminal S (inverter side), shown in Fig. 6, we have:

$v_s=v_{(+)}+v_{(-)}$ (20), $i_s=i_{(+)}-i_{(-)}$ (21),

$v_{(+)}=Z_0 i_{(+)}$ (22), $v_{(-)}=Z_0 i_{(-)}$ (23),

$v_s=V_0$ (24)

where v_s is the voltage of terminal S, $v_{(-)}(t)$ represents backward waves reflected from the motor end as in (18), while $v_{(+)}(t)$ represents the forward waves which comprise both the initiated forward wave from the inverter switching and the reflection of backward travelling waves at this terminal. While the first backward wave $v_{(-1)}(t)$ arrives at the inverter side (terminal S) and the inverter output voltage $v_s(t)$ stays at V_o as shown in Fig.1 (a), we have:

$v_{(-)}=v_{(-1)}$ (25), $v_{(+)}=v_s(t)+v_{(+1)}$ (26),

and

$v_s(t)=V_0$ (27).

Substituting (25), (26) and (27) into (20) the result is:

$v_{(+1)}=-v_{(-1)}$ (28)

The second incident wave (28) with its opposite slope causes a discharging process for the termination capacitance turning the increasing terminal voltage downward. Consequently, a criterion can be derived, where the maximum terminal voltage appears to be based on the charging voltage curve, e.g. (19), as determined by the period a wave travels back and forth along the cable. It follows that the longer the cable, the longer wave travel time is needed to result in the higher voltage ramp up. In addition, larger capacitance slows the rate of voltage ramp resulting in a lower maximum voltage for a given length of cable. The experimental voltage waveforms, as in Fig. 5 manifest the effects of motor parameters on maximum terminal voltage, which confirm the analytical exponential waveform.

The reflection of traveling waves at two ends of the cable yields consecutive traveling waves in opposite traveling direction as aforementioned. These waves may be solved by using either equations (4) to (8) or (20) to (24), respectively, with corresponding initial conditions. In view of this, it is possible that the maximum voltage of terminal A may exceed two units of V_0 under certain initial conditions, when $V_c(0)$ is not zero.

The voltage at any time and any location on the cable should be the sum of all the preceding waves, that is:

$v=v_{(+)}+v_{(-)}$ (29)

where

$v_{(+)}=v_s(t)+v_{(+1)}+v_{(+2)}+\ldots.$ (30)

$v_{(-)}=v_{(-1)}+v_{(-2)}+v_{(-3)}+\ldots..$ (31)

Based on above observation the voltage distribution may be simply illustrated in Fig. 8 where the cable length is assumed to be sufficiently long so that the delay time of the cable is much greater than the pulse rise-time.

4. RINGING TRANSIENT OF TERMINAL VOLTAGE

Through the above discussion it would seem that the reflection phenomenon should continue causing voltage oscillations with the frequency depending on the travel time of the wave. However, such expected frequencies do not agree with those observed, e.g. in Fig. 5. A hypothesis is thus proposed that the transient consists of two consecutive elements. The first element (as discussed above) is where the cable functions as a transmission line, and the motor surge impedance is dominated by its capacitance-resistance parameters. As analyzed in section 3, the reflection wave $v_{(-1)}$ at the motor terminal has a lower slope compared to the incident wave $v_{(+)}(t)$ due to the charging capacitance of the motor. This results in a progressively decreasing slope dv/dt of the wave front. This eventually leads to the second mode where the variance of shunt current through stray capacitance in the cable can be omitted. Therefore, the cable may be modeled as a "lumped inductance-capacitance" circuit, whereas the motor be a capacitance-resistance circuit. Damping oscillations (ringing) is the second stage of the transient. In practice, most transient ringing is in the frequency range of hundreds of kHz. These frequencies are far higher than typical motor resonant frequencies but still much lower than the characteristic frequency of the cable which occurs when the corresponding quarter wave length equals the cable length.

In addition to the experimental frequency response as shown in Fig. 2 the observation of the changes in the cable

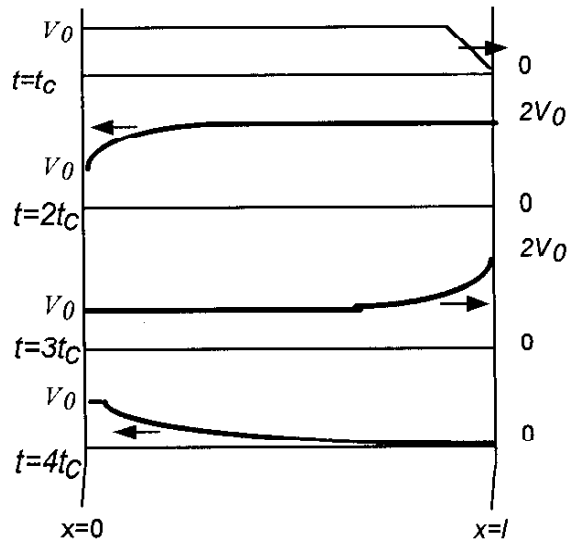

Fig. 8 Voltage distribution along cable due to reflection of travel wave at terminals. l is the length of cable, t_c the cable's delay time, V_0 the inverter pulse magnitude

model can be verified analytically by means of integrating the transmission line equations (1a) from $x=0$ to $x=l$, and leaving out the voltage derivative terms (higher than the third order) because of the decreasing dv/dt. The integration of (1a) is shown in (32) and then (33) is as follows:

$$\int_0^l \frac{\partial v}{\partial x} dx = -\int_0^l L_0 \frac{\partial i}{\partial t} dx \qquad (32)$$

$$v_s - v_a = L_l \frac{di_a}{dt} + \frac{L_l}{2}\frac{d}{dt}(C_l \frac{dv_a}{dt}) \qquad (33)$$

where l is the length of cable, and v_s, i_s, v_a, i_a are the voltage and current at terminal A and terminal S respectively. The quantities L_l and C_l are the entire inductance and capacitance of the cable with a length of l. The equivalent circuit of (33) is known as the pi type circuit as shown in Fig. 9. Similarly, integration of (1b) can lead to the known T type equivalent circuit for cable.

The transient voltage during the second stage can be analyzed on the basis of a "lumped circuit" model for any inverter-cable-motor system. The initial conditions at the second stage are determined from the previous stage. Therefore, the motor's characteristics contribute to the system transient, including the ringing as evidenced in Fig. 5. The entire transient voltage should consist of a number of frequency components, which depend on termination and cable characteristic frequencies. Fig. 10 is the spectrum of a 2.2 kW motor terminal voltage showing ringing frequency of 780 kHz and a number of sub-peaks.

5. R-C Network Termination

An *R-C* network terminator has already been demonstrated as a cost-effective solution to control over-voltage for many drive systems [6]. To date, previous designs have been based on "impedance matching". The resistance is selected to match the surge impedance of the cable. The capacitance is selected to maintain voltage below a certain level at the end of the rise time of the inverter pulse. In this paper a different design criteria is proposed as follows: 1) The capacitor C is added to the terminal with its selection based on the time constant $C(R+Z0)$ to slow down the rate of charging. This results in a lower maximum voltage for a given period, which depends on the time the reflection wave returns through the cable. 2) The resistor R is connected in series with C offering an additional damping factor. There is an optimal value for selection of C in a given system. 3) Heat consumption of resistance R depends upon the energy stored in the capacitance, $(1/2)CV^2$ and the charge/discharge rate (switching frequency). The *R-C* network is especially well suited for drive system applications with a low switching frequency, small or medium size motor and a short to medium cable length. Experimental results from both lab experiments and industrial field installations confirm this idea as in Fig. 11.

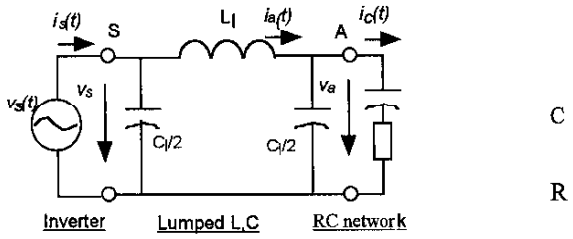

Fig. 9 Simplified inverter-cable-motor drive model 2.

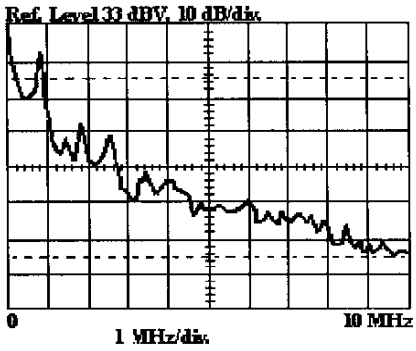

Fig. 10 Experimental spectrum of motor terminal voltage, 2.2 kW motor fed by 230 V inverter via 45 meter cable.

6. Conclusions

1) In modern drive systems the output voltage frequency band reaches up to the MHz range. At this point, the motor model behaves more like an *L-R-C* network than a simple *L-R* network and the cable must be modeled both as "distributed parameters" of the transmission line and a "*LCR* lumped" circuit based on the time order.

2) In most drive systems (since neither the magnitude nor phase angle of the motor impedance match the surge impedance of cable), the incident wave initiated from the inverter (arriving at the motor terminal) will first charge the stray capacitance of the motor winding causing a reflection wave backward along the cable. The terminal voltage will ramp up roughly exponentially. The over-voltage is first determined by the charging rate and the charging period. These phenomena are related to the rise time of the incident wave, capacitance and resistance of the

terminator, cable characteristics (including wave propagation velocity and the length of the cable) and surge impedance.

3) As the signal *dv/dt* decreases (through wave propagation and reflection) the cable behavior changes from "distributed parameters" to "lumped inductance-capacitance circuit", in conjunction with the termination circuit which governs the ongoing transient as in a ringing stage.

4) Regarding the artificial *RC* network design the capacitance of the *RC* network is selected to slow down the voltage charging rate which controls the amplitude of over-voltage. The capacitance also causes heat consumption problems. The resistance of the *RC* network offers the necessary damping of which there is an optimal value of *R* for the selected *C* in a given system, e.g. in Fig. 9.

ACKNOWLEDGMENT

The authors would like to acknowledge the Wisconsin Electric Machines and Power Electronics Consortium (WEMPEC) for generously offering the facility and opportunity to complete most of the experiments referenced in this paper.

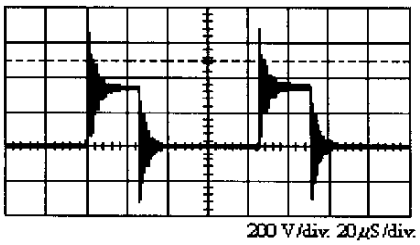

(a)

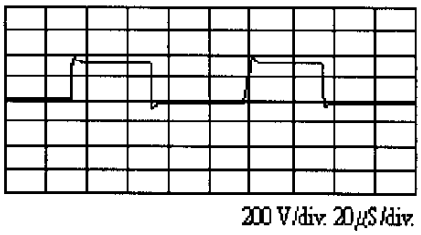

(b)

Fig. 11 Experimental waveform of 2.2 kW motor, fed by 230 V inverter via 45 meter cable: (a) without compensation, (b) with RC terminator (R130 Ω C0.01 μF)

REFERENCES

[1] E. Person, "Transient effects in application of PWM inverter to induction motors," *IEEE Trans. Ind. Appl. Vol.28, No.5, Sep/Oct. 1992.*

[2] R. H. Daugherly and C. H. Wennerstrom, "Need for industry standards for ac induction motors intended for use with adjustable-frequency controllers," *IEEE Ind. Appl. Vol.27. No.6. Nov/Dec. 1991.*

[3] D.B. Hyypio, "Simulation of cable and winding response to steep-fronted voltage waves," *IEEE IAS Conference Proceedings, 1995, pp. 800-806.*

[4] P. V. Poucke, R. Belmans, W. Geysen, and E. Ternier, "Overvoltages in inverter fed induction machines using high frequency power electronic components," *IEEE APEC Proceedings, 1994, pp.536-541.*

[5] A. V. Jouanne, P. Enjeti, and W. Gray, "The effect of long motor leads on PWM inverter fed AC Motor Drive Systems," *IEEE APEC Conference Proceedings,1995, pp.579-585.*

[6] G. Skibinski "Design methodology of a cable terminator to reduce reflected voltage on AC motors," *IEEE IAS Conference Proceedings, 1996.*

[7] Chingchi Chen, Xingyi Xu, "Loss-less & cost-effective cable terminator topologies with no voltage overshoot," *IEEE APEC Conference Proceedings, 1998, pp. 1030-1034.*

[8] R. Kerkman, D. Leggate, and G. Skibinski, "Interaction of drive modulation & cable parameters on AC motor transients," *IEEE IAS Conference Proceedings, 1996.*

[9] Y. Murai, T. Kubota, and Y. Kawase, "Leakage current reduction for a high-frequency carrier inverter feeding an induction motor," *IEEE Trans. Ind. Appl.*, vol. 28, no 4, *pp.* 858-863 Jul/Aug. 1992.

[10] S. Ogasawara and H. Akagi, "Modeling and damping of high-frequency leakage currents in PWM inverter-fed AC motor drive systems," *IEEE Trans. Ind. Appl.*, vol. 32, no 6, *pp.* 1105-1114, Sep./Oct..1996.

[11] D. Maly, D. W. Novotny, and C. Thompson, "The influence of winding capacitance on high frequency time harmonic losses in induction motors," *IEEE IAS Conference Proceedings, 1992, pp. 33-39.*

[12] Shaotang Chen, T.A. Lipo, and D. Fitzgerald, " Modeling of motor bearing currents in PWM inverter drives," *IEEE Trans. Ind. Appl.*, vol. 32, no 6, *pp.* 1365-1370, Nov/Dec. 1996.

[13] Erkuan Zhong, T.A. Lipo, "Improvements in EMC performance of inverter-fed motor drives" *IEEE Trans. Ind. Appl.*, vol. 31, no. 6, Nov./Dec. 1995.

[14] Erkuan Zhong, T.A. Lipo, J.R. Jaeschke, and D. Gritter, "Analytical estimation and reduction of conducted EMI emissions in high power PWM inverter drives," *IEEE PESC Conference Proceedings, 1996, pp.1169-1175.*